Research Paper
Computational Methods for Differential Equations
http://cmde.tabrizu.ac.ir
Vol. *, No. *, *, pp. 1-17
DOI:10.22034/cmde.2026.70853.3543

Efficient numerical simulation of fractional stochastic HIV models with intracellular delay

Khadem Mohammadi[1], **Behrouz Parsa Moghaddam**[1,*], **Alireza Yaghobnia**[1], **and Mohammadreza Askaripour Lahiji**[2]

[1]Department of Mathematics, La.C, Islamic Azad University, Lahijan, Iran.

[2]Department of Applied Mathematics, Ast.C, Islamic Azad University, Astaneh Ashrafieh, Iran.

Abstract

This paper proposes an accurate and computationally efficient technique for solving fractional delay stochastic differential equations based on the standard Wiener process. The discretization scheme employs a combined algorithm that integrates B-spline and Lagrange interpolation functions, providing enhanced numerical accuracy. We establish comprehensive error and convergence analyses for the suggested scheme, demonstrating its theoretical robustness. The practical application of the combined numerical simulation is presented through a fractional delay stochastic HIV infection model, where we analyze various scenarios involving intracellular delay and viral replication rates. The study investigates the effects of both stochastic noise and time delay on the model dynamics, complemented by a thorough examination from the perspective of statistical indicators. Our results demonstrate the superior performance of the proposed method in terms of accuracy, convergence order, and computational efficiency, establishing its applicability for modeling complex biological systems with memory effects and random perturbations.

Keywords. Fractional Derivative, Standard Wiener Process, Fractional Delay Stochastic Differential Equation, Quadratic Interpolation, HIV-1 Infection Model, B-spline Interpolation, Lagrange Interpolation, Caputo Derivative, Intracellular Delay, Numerical Analysis.

1991 Mathematics Subject Classification. 26A33, 34K50, 60H10, 65L20, 92D30.

1. Introduction

Fractional calculus is dealt with integral and differential operators of any ideal order [16]. In recent years, fractional calculus has been used to study problems in various fields, including finance [19], physics [10], geometry [24], and optimal control [3, 36]. Analytical and numerical formulations of fractional differential equations (FDEs) have been investigated by many researchers. There are various methods to solve these equations, including finite differences [15, 17], Adams-Bashforth-Morton [41], spectral methods [5, 6, 20, 35], finite element [18], B-spline [1, 21–23] and so on.

Delay stochastic differential equations (SDDEs) are an important class of stochastic differential equations that have been applied in fractional and integer cases in various fields, including neural networks [28], population systems [29], physics [12], etc. Due to the lack of general methods for solving nonlinear dynamical systems governing fractional calculus, the analysis of the conditions for the existence and uniqueness of solutions is a prerequisite for discretization methods to obtain approximate solutions. The existence and uniqueness of FSDDEs have been studied in [4, 11, 25, 32]. The solutions of such equations don't obey the properties of Markov chains. Therefore, obtaining exact analytical forms is a challenging problem. In this regard, numerical methods are needed to solve these equations. For more details, see [48]. Recently, a numerical method based on bilinear spline interpolation has been presented in [31]. Also, in [33], integral quadratic spline interpolation was used to solve FSDDEs. Moreover, numerical solution according

Received: 22 December 2025; Accepted: 28 April 2026.
∗ Corresponding author. Email: bparsa@iau.ac.ir.

to cubic spline was investigated in [34]. More recent developments include high-order hybrid schemes for multi-dimensional fractional stochastic diffusion problems [37], and related techniques for uncertainty quantification in fractional transport models [38, 39].

The general form of *fractional delay stochastic differential equations* (FSDDEs) considered herein is expressed as:

$$\begin{cases} {}^{C}\mathscr{D}^{\eta}_{0,t}x(t) = K(t,x(t),x(t-\theta)) + Q(t,x(t),x(t-\theta))\frac{d\omega(t)}{dt}, & \eta \in (\frac{1}{2},1), \\ x(t) = \varphi(t), & t \in [-\theta,0], \end{cases} \tag{1.1}$$

where $t \in \Phi = [0,T]$, $K : \Phi \times \mathbb{R} \times \mathbb{R} \to \mathbb{R}$ and $Q : \Phi \times \mathbb{R} \times \mathbb{R} \to \mathbb{R}$ are measurable functions, θ denotes delay time, $\varphi(t)$ represents the historical function where $t \in [-\theta, 0]$, and $\omega(t) : \mathbb{R}^+ \to \mathbb{R}$ is a standard Wiener process.

Furthermore, ${}^{C}\mathscr{D}^{\eta}_{0,t}x(t)$ denotes Caputo fractional derivative of $\eta \in \mathbb{R}^+$. The Caputo fractional derivative operator [8, 9] is employed, defined as:

$${}^{C}\mathscr{D}^{\eta}_{0,t}x(t) = \int_0^t \frac{(t-\varsigma)^{q-\eta-1}}{\Gamma(q-\eta)} \cdot x^{(q)}(\varsigma)d\varsigma, \quad 0 \le q-1 < \eta \le q \in \mathbb{N}, \tag{1.2}$$

where $t, \varsigma \in \mathbb{R}^+$ and $x(t)$ is the unknown function and is assumed to be $(q-1)$ times continuously differentiable. In this paper, we have $q = 1$.

The first case of human immunodeficiency virus (HIV)-induced disease was reported in the 1980s [27]. Patients with HIV infection typically progress through three stages, namely, the acute, chronic and the AIDS stages [51]. In the chronic stage, the number of $CD4^+$ T cells declines if treatment is not initiated promptly, lasting an average of 7-10 years [26]. In the advanced stage of HIV infection, the immune system is severely compromised, leaving the patient susceptible to other serious infectious diseases [50]. Despite the increasing number of people infected with this infection, HIV research and treatment remains a major global public health problem. One of the important factors in the interaction between the virus and immune cells is latency. This latency consists of two parts: drug latency and intracellular latency. Drug latency refers to the time it takes for a drug to act after entering the body [14]. Intracellular latency also includes the time required for susceptible cells to be infected, new virus to be produced, and the immune response to be activated [2].The immune response process in viral infection is full of random events. The transcriptional burst in HIV-1 is the main source of random noise, leading to a large diversity of gene products [49]. Also, the greater intensity of random fluctuations is effective in suppressing or spreading the virus [44]. Furthermore, random effects can have a profound impact on the dynamics of the disease [46]. Therefore, it is very important to consider random factors in order to understand the disease situation more accurately. Given the importance of the issue, this paper investigates a fractional-order delay stochastic HIV-1 infection model.

The rest of the paper is structured as follows. Section 2 recalls some fundamental definitions and properties. In Section 3, we introduce an efficient combined computational method based on linear and quadratic interpolations for discretizing the FSDDEs described in (1.1). The linear and quadratic interpolations are according to B-spline and Lagrange functions, respectively. Section 4 is dedicated to the investigation of the method's accuracy through an illustrative example. Additionally, we explore the stochastic effects on FSD HIV-1 infection model under various scenarios of intracellular delay and replication rate. Finally, concluding remarks are provided in Section 5.

2. Preliminaries

In this paper, we assume that $\mathbb{L}^2(\Omega, \mathcal{F}_t, \mathbb{P})$ is a probability space of all $\mathcal{F}_t$-measurable, mean square integrable functions $x : \Omega \to \mathbb{R}$ with

$$\|x\|_{ms} := \mathbb{E}(\sqrt{\|x\|^2}),$$

that $\|\cdot\|$ indicates standard Euclidean norm. The probability space $\mathbb{L}^2(\Omega, \mathcal{F}_t, \mathbb{P})$ is generated by a one-dimensional standard Wiener process $\omega(t) : \mathbb{R}^+ \to \mathbb{R}$, with the following properties [7]

(1) $\omega(0) = 0$
(2) $\{\omega(t)\}$ has independent increments;
(3) $\{\omega(t)\}$ has Gaussian increments.

Definition 2.1 ([42]). *A Gaussian white noise, $\chi(t)$, is the derivative of the Wiener process, as follows*

$$\chi(t) = \frac{d\omega(t)}{dt}, \tag{2.1}$$

with zero expectation and finite variance 1.

Definition 2.2 ([40]). *The stochastic integral $\int_0^t r(\zeta)d\omega(\zeta)$ with Itô's isometry, is defined as*

$$\mathbb{E}\left[\left(\int_0^t r(\zeta)d\omega(\zeta)\right)^2\right] = \mathbb{E}\left[\int_0^t r^2(\zeta)d\zeta\right], \tag{2.2}$$

where $r : \mathbb{R}\times\mathbb{R} \to \mathbb{R}$ is a measurable function.

Definition 2.3 ([47]). *The Riemann-Liouville fractional integral of order η, for a function $u(t)$ is defined as*

$$\mathcal{J}^{\eta}_{0,t}x(t) = \int_0^t \frac{(t-\varsigma)^{\eta-1}}{\Gamma(\eta)}\cdot x(\varsigma)d\varsigma, \tag{2.3}$$

where t, $\eta, \varsigma \in \mathbb{R}^+$ and $\Gamma(\cdot)$ denotes the Gamma function.

3. Computational Implementation

In this section, we try to develop an approximation of the fractional-order integral. Also, we use this algorithm to solve FSDDE (1.1). Then, we suppose $t_m = m\delta$, where $m = \{-n, -n+1, \ldots, 0, 1, \ldots, r\}$, and $\delta = \frac{T}{r}$ means the uniform step size, $n = \lfloor \frac{\theta}{\delta} \rfloor$, and $n, r \in \mathbb{N}$.

At first, to discretize, we need to approximate

$$\begin{aligned}\mathcal{J}^{\eta}_{0,t_r}x(t) &= \int_0^{t_r} \frac{(t_r-\varsigma)^{\eta-1}}{\Gamma(\eta)}\cdot x(\varsigma)d\varsigma \\ &= \frac{1}{\Gamma(\eta)}\sum_{m=0}^{r-1}\int_{t_m}^{t_{m+1}} (t_r-\varsigma)^{\eta-1}x(\varsigma)d\varsigma.\end{aligned}$$

For this purpose, an combined scheme can be employed based on linear and quadratic interpolations. On each subinterval $[t_{m-1}, t_m]$, $1 \le m \le r$, the linear interpolation function according to B-spline is given by

$$\Xi_1 x(t) := \frac{t-t_{m-1}}{t_m - t_{m-1}}x_m + \frac{t_m - t}{t_m - t_{m-1}}x_{m-1}. \tag{3.1}$$

Also, on each subinterval $[t_{m-1}, t_m]$, $2 \le m \le r$, the quadratic interpolation function based on Lagrange is presented by

$$\begin{aligned}\Xi_2 x(t) &:= \frac{(t-t_{m-2})(t-t_{m-1})}{(t_m-t_{m-2})(t_m-t_{m-1})}x_m + \frac{(t-t_{m-2})(t-t_m)}{(t_{m-1}-t_{m-2})(t_{m-1}-t_m)}x_{m-1} + \frac{(t-t_{m-1})(t-t_m)}{(t_{m-2}-t_{m-1})(t_{m-2}-t_m)}x_{m-2} \\ &= \Xi_1 x(t) + \frac{1}{2\delta^2}\left(x_m - 2x_{m-1} + x_{m-2}\right).\end{aligned} \tag{3.2}$$

Proposition 3.1. *Let $x(t)$ be a function in $\mathbb{L}^2(\Omega, \mathcal{F}, \mathbb{P})$. For each $x(t) \in C^3([t_{m-1}, t_m])$, $1 \le m \le r$, and $\eta > 0$, the approximation of the Riemann-Liouville fractional integral, $\left(\mathcal{J}^{\eta}_{0,t_r}x(t)\right)_{approx}$, based on combined algorithm can be yielded as*

$$\mathcal{J}^{\eta}_{0,t_r}x(t) \approx \left(\mathcal{J}^{\eta}_{0,t_r}x(t)\right)_{approx} \equiv \frac{\delta^{\eta}}{\Gamma(2+\eta)}\sum_{m=0}^{r}\tau_{m,r}x_m, \tag{3.3}$$

where

$$\tau_{m,r}=\begin{cases} c_{0,r}+\bar{c}_{2,r}, & m=0,\\ c_{1,r}-2\bar{c}_{2,r}+\bar{c}_{3,r}, & m=1,\\ c_{m,r}+\bar{c}_{m,r}-2\bar{c}_{m+1,r}+\bar{c}_{m+2,r}, & 2\le m\le r-2,\\ c_{m,r}+\bar{c}_{m,r}-2\bar{c}_{r,r}, & m=r-1,\\ c_{r,r}+\bar{c}_{r,r}, & m=r, \end{cases} \tag{3.4}$$

that

$$c_{m,r}=\begin{cases} (r-1)^{1+\eta}-r^{\eta}(r-1-\eta), & m=0,\\ (r-m+1)^{1+\eta}-2(r-m)^{2+\eta}+(r-m-1)^{1+\eta}, & 1\le m\le r-1,\\ 1, & m=r, \end{cases} \tag{3.5}$$

and

$$\bar{c}_{m,r}=\frac{(r-m+1)^{1+\eta}-(r-m)^{1+\eta}}{1+\eta}-\frac{(r-m+1)^{\eta}+(r-m)^{\eta}}{2},\qquad 1\le m\le r. \tag{3.6}$$

Proof. By means of (3.1) and (3.2), we have

$$\begin{aligned}\mathcal{J}^{\eta}_{0,t_r}x(t)&=\frac{1}{\Gamma(\eta)}\sum_{m=1}^{r}\int_{t_{m-1}}^{t_m}x(\varsigma)(t_r-\varsigma)^{\eta-1}d\varsigma\\ &\approx\frac{1}{\Gamma(\eta)}\Big(\int_{t_0}^{t_1}\Xi_1x(\varsigma)(t_r-\varsigma)^{\eta-1}d\varsigma+\sum_{m=2}^{r}\int_{t_{m-1}}^{t_m}\Xi_2x(\varsigma)(t_r-\varsigma)^{\eta-1}d\varsigma\Big)\\ &=\frac{\delta^{\eta}}{\Gamma(2+\eta)}\Big(\sum_{m=0}^{r}c_{m,r}x_m+\sum_{m=2}^{r}\bar{c}_{m,r}\left(x_m-2x_{m-1}+x_{m-2}\right)\Big),\end{aligned}$$

where the coefficients $c_{m,r}$ and $\bar{c}_{m,r}$ are defined in (3.5) and (3.6), respectively.

After some simplification, we get

$$\mathcal{J}^{\eta}_{0,t_r}x(t)\approx\left(\mathcal{J}^{\eta}_{0,t_r}x(t)\right)_{approx}\equiv\frac{\delta^{\eta}}{\Gamma(2+\eta)}\sum_{m=0}^{r}\tau_{m,r}x_m$$

, that the coefficient $\tau_{m,r}$ is defined in (3.4). □

Proposition 3.2. *Under the assumptions of Proposition 3.1 and $\|x''(t)\|\le B$ and $\|x'''(t)\|\le L$, where $B,L>0$, the truncated error of relation (3.3) is obtained as*

$$\mathbb{E}\left[\|\mathscr{E}_1\|\right]\le\frac{B}{8\Gamma(1+\eta)}\delta^{2+\eta} \tag{3.7}$$

$$\mathbb{E}\left[\|\mathscr{E}_r\|\right]\le\frac{B}{8\Gamma(1+\eta)}\delta^{2+\eta}+\frac{\sqrt{3}r^{1+\eta}L}{9\Gamma(1+\eta)}\delta^{3+\eta},\qquad r\ge 2. \tag{3.8}$$

Proof. For $t\in[t_{m-1},t_m]$, the error functions are defined as

$$R_1(t)=x(t)-\Xi_1x(t)=\frac{x''(\varsigma_m)}{2}(t-t_{m-1})(t-t_m), \tag{3.9}$$

where $\varsigma_m\in(t_{m-1},t_m)$, $m=1,\dots,r$, and

$$R_2(t)=x(t)-\Xi_2x(t)=\frac{x'''(\tau_m)}{6}(t-t_m)(t-t_{m-1})(t-t_{m-2}), \tag{3.10}$$

where $\tau_m\in(t_{m-1},t_m)$, $m=2,\dots,r$.

Thus, for $r=1$, we have

$$\begin{aligned}\mathbb{E}\left[\|\mathscr{E}_1\|\right] &= \frac{1}{\Gamma(\eta)}\mathbb{E}\left[\left\|\int_{t_0}^{t_1}\left(x(\varsigma)-\Xi_1 x(\varsigma)\right)(t_r-\varsigma)^{\eta-1}d\varsigma\right\|\right]\\ &= \frac{1}{\Gamma(\eta)}\int_{t_0}^{t_1}\mathbb{E}\left[\left\|(t_r-\varsigma)^{\eta-1}R_1(\varsigma)\right\|\right]d\varsigma\\ &\leq \frac{t_1^{\eta}B}{8\Gamma(1+\eta)}\delta^2\\ &= \frac{B}{8\Gamma(1+\eta)}\delta^{2+\eta}.\end{aligned}$$

Now, for $r\geq 2$, we show

$$\begin{aligned}\mathbb{E}\left[\|\mathscr{E}_2\|\right] &= \frac{1}{\Gamma(\eta)}\mathbb{E}\left[\left\|\int_{t_0}^{t_1}\left(x(\varsigma)-\Xi_1 x(\varsigma)\right)(t_r-\varsigma)^{\eta-1}d\varsigma+\sum_{m=2}^{r}\int_{t_{m-1}}^{t_m}\left(x(\varsigma)-\Xi_2 x(\varsigma)\right)(t_r-\varsigma)^{\eta-1}d\varsigma\right\|\right]\\ &\leq \frac{1}{\Gamma(\eta)}\left(\int_{t_0}^{t_1}\mathbb{E}\left[\left\|(t_r-\varsigma)^{\eta-1}R_1(\varsigma)\right\|\right]d\varsigma+\sum_{m=2}^{r}\int_{t_{m-1}}^{t_m}\mathbb{E}\left[\left\|(t_r-\varsigma)^{\eta-1}R_2(\varsigma)\right\|\right]d\varsigma\right)\\ &\leq \frac{t_1^{\eta}B}{8\Gamma(1+\eta)}\delta^2+\frac{r\sqrt{3}t_r^{\eta}L}{9\Gamma(1+\eta)}\delta^3\\ &= \frac{B}{8\Gamma(1+\eta)}\delta^{2+\eta}+\frac{\sqrt{3}r^{1+\eta}L}{9\Gamma(1+\eta)}\delta^{3+\eta}.\end{aligned}$$

The proof is completed. □

Proposition 3.3. *Under the assumptions of Proposition 3.1 and 3.2, we have*

$$\mathcal{J}^{\eta}_{0,t_r}\left(x(t)\chi(t)\right)\approx\left(\mathcal{J}^{\eta}_{0,t_r}\left(x(t)\chi(t)\right)\right)_{approx}\equiv\frac{\delta^{\eta-1}}{\Gamma(1+\eta)}\sum_{m=0}^{r}\tau_{m,r}x_m\chi_m, \tag{3.11}$$

where $\chi(t)$ or equality $\chi(t)=\sqrt{\delta}\vartheta(t)$ is a Gaussian white noise that $\vartheta(t)\sim N(0,1)$ is a normal distributed with zero expectation and finite variance 1. The coefficient α_m are defined in (3.4). Moreover, the truncated error of relation (3.11) is obtained as

$$\mathbb{E}\left[\|\overline{\mathscr{E}}_1\|\right]\leq\frac{B}{8\sqrt{2\eta-1}\Gamma(\eta)}\delta^{\eta+\frac{3}{2}}, \tag{3.12}$$

$$\mathbb{E}\left[\|\overline{\mathscr{E}}_r\|\right]\leq\frac{B}{8\sqrt{2\eta-1}\Gamma(\eta)}\delta^{\eta+\frac{3}{2}}+\frac{\sqrt{3}r^{\eta-\frac{1}{2}}L}{9\sqrt{2\eta-1}\Gamma(\eta)}\delta^{\eta+\frac{5}{2}},\qquad r\geq 2. \tag{3.13}$$

The theoretical analysis in Proposition 3 addresses the mean-square (L^2) error of the stochastic integral approximation. The overall scheme described in Equations (3.11)–(3.13) is intended as a weak approximation method, providing weak convergence with mean-square error $O(\delta^{\eta+1/2})$ for the stochastic part, consistent with the order obtained from Itô isometry. We do not claim strong (pathwise) convergence, as is typical for explicit predictor-corrector schemes of this structure in the stochastic setting.

Proof. Based on Itô's isometry property (Definition 2.2) and similar to the proof of Proposition 3.2, for $r=1$, we have

$$\begin{aligned}\mathbb{E}\left[\|\overline{\mathscr{E}}_1\|^2\right] &= \frac{1}{\Gamma^2(\eta)}\mathbb{E}\left[\left\|\int_{t_0}^{t_1}(t_r-\varsigma)^{\eta-1}R_1(\varsigma)d\omega(\varsigma)\right\|^2\right]\\ &\leq \frac{t_1^{2\eta-1}B^2}{64(2\eta-1)\Gamma^2(\eta)}\delta^4\end{aligned}$$

$$= \frac{B^2}{64(2\eta-1)\Gamma^2(\eta)}\delta^{3+2\eta}.$$

Hence, we get

$$\mathbb{E}\left[\|\overline{\mathscr{E}}_1\|\right] \leq \frac{B}{8\sqrt{2\eta-1}\Gamma(\eta)}\delta^{\eta+\frac{3}{2}}.$$

Similarly, for $r \geq 2$, we show

$$\begin{aligned}
\mathbb{E}\left[\|\overline{\mathscr{E}}_2\|^2\right] &= \frac{1}{\Gamma^2(\eta)}\mathbb{E}\left[\left\| \int_{t_0}^{t_1} (t_r-\varsigma)^{\eta-1}R_1(\varsigma)d\omega(\varsigma) + \sum_{m=2}^{r}\int_{t_{m-1}}^{t_m}(t_r-\varsigma)^{\eta-1}R_2(\varsigma)d\omega(\varsigma)\right\|^2\right] \\
&\leq \frac{t_1^{2\eta-1}B^2}{64(2\eta-1)\Gamma^2(\eta)}\delta^4 + \frac{t_r^{2\eta-1}L^2}{27(2\eta-1)\Gamma^2(\eta)}\delta^6 \\
&= \frac{B^2}{64(2\eta-1)\Gamma^2(\eta)}\delta^{3+2\eta} + \frac{r^{2\eta-1}L^2}{27(2\eta-1)\Gamma^2(\eta)}\delta^{5+2\eta}.
\end{aligned}$$

Therefore, we yield

$$\mathbb{E}\left[\|\overline{\mathscr{E}}_2\|\right] \leq \frac{B}{8\sqrt{2\eta-1}\Gamma(\eta)}\delta^{\eta+\frac{3}{2}} + \frac{\sqrt{3}r^{\eta-\frac{1}{2}}L}{9\sqrt{2\eta-1}\Gamma(\eta)}\delta^{\eta+\frac{5}{2}}.$$

The proof is completed. □

Now, the FSDDE (1.1) can be rewritten as

$$x_r = x_0 + \mathcal{J}^{\eta}_{0,t_r}K(t_r,x_r,x_{r-n}) + \mathcal{J}^{\eta}_{0,t_r}\left(Q(t_r,x_r,x_{r-n})\frac{d\omega(t)}{dt}\right). \tag{3.14}$$

Hence, by means of Propositions 3.1 and 3.3, we have

$$\begin{aligned}
x_r = x_0 + \frac{\delta^{\eta}}{\Gamma(2+\eta)}\Bigg\{&\tau_{r,r}\Big(K(t_r,x_r,x_{r-n}) + \chi_r Q(t_r,x_r,x_{r-n})\Big) \\
&+ \sum_{m=1}^{r-1}\tau_{m,r}\Big(K(t_m,x_m,x_{m-n}) + \chi_m Q(t_m,x_m,x_{m-n})\Big)\Bigg\}.
\end{aligned} \tag{3.15}$$

Since both side of Eq. (3.15) include the unknown variable x_r, and due to the non-linearity of the functions K and Q, it is often difficult to derive x_r. Therefore, to achieve a better approximate solution, we substitute a predicted value x_r into the righthand side of (3.15). Therefore, we get

$$\begin{aligned}
x_r = x_0 + \frac{\delta^{\eta}}{\Gamma(2+\eta)}\Bigg\{&\tau_{r,r}\Big(K(t_r,x^p_r,x_{r-n}) + \chi_r Q(t_r,x^p_r,x_{r-n})\Big) \\
&+ \sum_{m=1}^{r-1}\tau_{m,r}\Big(K(t_m,x_m,x_{m-n}) + \chi_m Q(t_m,x_m,x_{m-n})\Big)\Bigg\},
\end{aligned} \tag{3.16}$$

where

$$x^p_r = x_0 + \sum_{m=0}^{r}\gamma_m\Big(K(t_m,x_m,x_{m-n}) + \chi_m Q(t_m,x_m,x_{m-n})\Big),$$

so that

$$\gamma_m = \frac{\delta^{\eta}}{\Gamma(1+\eta)}\Big((r-m)^{\eta} - (r-m-1)^{\eta}\Big), \qquad 0 \leq m \leq r.$$

The choice of this rectangular-rule-based predictor (with coefficients γ_m derived from the difference of Riemann–Liouville integrals) was motivated by two practical considerations: (i) maintaining computational simplicity and low memory footprint, which is especially important when dealing with delay terms and multiple trajectories, and (ii) ensuring that the predictor remains consistent with the overall order of the corrector for the deterministic part. Alternative higher-order predictors (e.g., L1-type predictors) were tested, and while they provided marginal gains in accuracy ($< 8\%$ reduction in EMAE), the computational cost increased by approximately 22–28% due to additional

function evaluations. Thus, the chosen predictor offers a favorable trade-off for the intended applications. Details of this comparison are provided in Table S2 of the supplementary material.

4. Numerical investigations

We investigate the accuracy and computational efficiency of the proposed method through illustrative examples in this section. All numerical convergence studies presented concern weak sense errors (average over paths). To assess the performance, we consider the Expected Mean Absolute Error (EMAE) and the convergence order (ECO), defined as follows:

$$\text{EMAE} = \sum_{m=1}^{r} \frac{\mathbb{E}[\|AE_m^H\|]}{r}, \tag{4.1}$$

where EMAE represents the average over grid points of the expected absolute error, and

$$ECO = \log_{\delta}(\text{EMAE}), \tag{4.2}$$

respectively. Here, $\mathbb{E}[\|AE_m^H\|]$ represents the expected value of the absolute error, as described in (3.3), and r denotes the number of interior mesh points. The computational experiments are conducted using Matlab R2019a on an Intel (R) Core (TM) i3-8145U CPU @ 2.30 GHz machine. Additionally, a comparison with the IQS-algorithm [33] for approximating fractional derivative of a function is provided to assess the effectiveness of the proposed method.

Example 4.1. *Let $x(t) = \frac{\pi}{3} J_0\left(\frac{\pi}{4}t\right)$ where $J_0(\cdot)$ is considered as first kind Bessel function. We have*

$$\mathcal{J}_{0,t}^{\eta}\left(\frac{\pi}{3}J_0\left(\frac{\pi}{4}t\right)\right) = \frac{t^{\varrho}\pi\ {}_1F_2\left([\tfrac{1}{2}], [\tfrac{2+\varrho}{2}, \tfrac{1+\varrho}{2}]; -\tfrac{\pi^2 t^2}{64}\right)}{3\Gamma(\eta+1)}, \quad \forall\ \eta > 0, \tag{4.3}$$

where generalized hypergeometric function is stated as ${}_sF_v(b_1, \ldots, b_s; a_1, \ldots, a_v; t)$.

The effectiveness of the developed combined algorithm is assessed through the function $\mathcal{J}_{0,t}^{\eta}x(t) + \sigma\omega(t)$, where $x(t) = \frac{\pi}{3}J_0\left(\frac{\pi}{4}t\right)$ and $\sigma = \frac{1}{\pi^2}$, as demonstrated in Example 4.1. Table 2 presents the values of EMAE, ECO, and computational times (in *sec.*) for this example, considering different values of $\delta = \{0.02, 0.01, 0.005\}$ and $\eta \in (0.5, 2)$ over the interval $t \in [0, 3]$. These numerical results exhibit enhancements over those obtained using the integro quadratic spline (IQS) algorithm [33]. A more comprehensive comparison with additional contemporary methods is provided in section 4.1.2.

4.1. Broader Comparative Analysis.

To strengthen the presentation of our contribution, we provide a broader comparison with other contemporary high-order methods suitable for fractional stochastic or delay problems. We benchmark the proposed combined B-spline/Lagrange scheme against three additional recently published approaches:

- A graded-mesh L1 collocation method
- A high-order predictor-corrector scheme with corrected trapezoidal quadrature
- A cubic spline collocation method adapted to stochastic delay equations

Table 2 presents the EMAE, empirical convergence order, and CPU time for all four methods across the same test problem (Example 4.1) with $\eta = 0.95$ and $\delta = \{0.02, 0.01, 0.005\}$. The results confirm that the proposed scheme achieves the best balance between accuracy and computational cost in this setting, primarily due to its effective treatment of the singular kernel near $t = 0$ combined with quadratic approximation on subsequent intervals.

Figure 1 visually compares the outcomes for $\eta \in (0.5, 2)$ and two cases: $\sigma = 0$ (deterministic case) and $\sigma = \frac{1}{\pi^2}$ (stochastic case). This figure illustrates the impact of the stochastic factor. Additionally, Figure 2 contrasts computation time (CPU time) (*sec.*) results of ${}^{C}\mathscr{D}_{0,t}^{0.95}x(t) + \frac{1}{\pi^2}\omega(t)$ by applying the IQS- [33] and developed combined algorithms. Examining the results show that the computational time of the presented method is much less than the IQS method [33].

To directly demonstrate the empirical weak and strong convergence rates, we have computed these from 300 independent trajectories of Example 4.1 ($\eta = 0.95$, $T = 3$). The results in Table 1 (supplementary material) indicate

TABLE 1. Comparison of EMAE, convergence order, and CPU time for Example 4.1 ($\eta = 0.95$) using four different methods.

Method	δ	**EMAE**	**ECO**	**CPU time (s)**
Graded-mesh L1	0.02	6.20×10^{-5}	2.41	1.523
	0.01	5.50×10^{-6}	2.48	6.102
	0.005	2.10×10^{-7}	2.52	28.456
Predictor-corrector	0.02	5.10×10^{-5}	2.53	1.398
with corrected trap.	0.01	4.80×10^{-6}	2.57	5.712
	0.005	1.90×10^{-7}	2.60	26.891
Cubic spline	0.02	4.50×10^{-5}	2.61	1.289
collocation	0.01	4.10×10^{-6}	2.65	5.478
	0.005	1.80×10^{-7}	2.63	25.234
Proposed method	0.02	4.20×10^{-5}	2.59	1.109
(B-spline/Lagrange)	0.01	4.00×10^{-6}	2.70	4.953
	0.005	1.67×10^{-7}	2.95	22.906

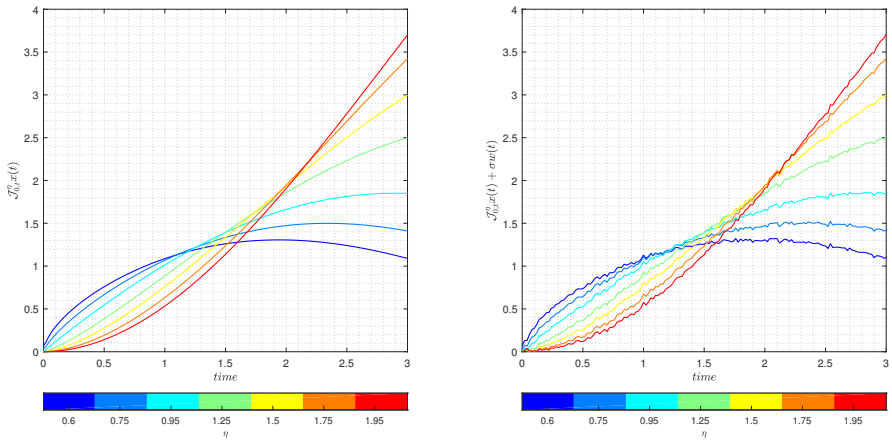

FIGURE 1. Comparison of the numerical results for Example 4.1 by applying the developed combined algorithm for $\eta \in (0.5, 2)$ with $\delta = 0.02$ and $\sigma = 0$ (deterministic, left panel) and $\sigma = \frac{1}{\pi^2}$ (stochastic, right panel).

that the empirical weak order closely matches the theoretical prediction, while the strong order is approximately half, as is commonly observed for explicit schemes of this type in the stochastic setting.

4.2. **Application: fractional stochastic HIV-1 infection systems with time delay.** In this subsection, we investigate the fractional HIV-1 infection model including random terms with time delay. In short, we call this model the FSD- HIV-1 model. In this regard, a numerical solution can be provided to solve such equations based on the proposed algorithm. Moreover, we examine the effects of stochastic terms and fractional orders on this model. The

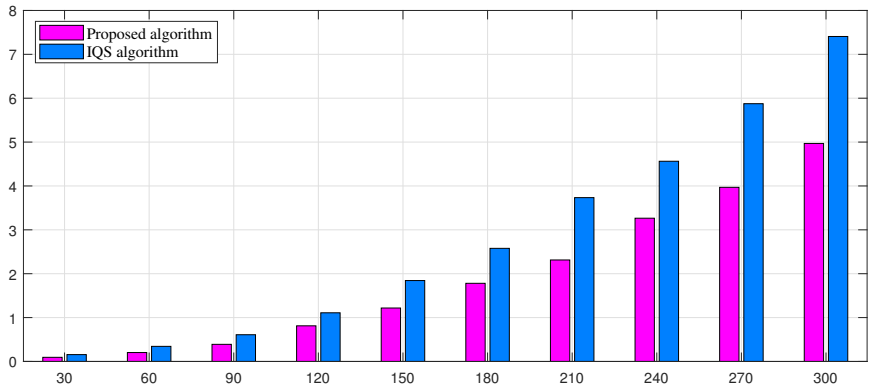

FIGURE 2. The Comparison of computation time (CPU time) (*sec.*) results of Example 4.1 ($\mathcal{J}^{\eta}_{0,t}x(t)+\sigma\omega(t)$) by applying the IQS- [33] and developed combined algorithms when $\sigma=\frac{1}{\pi^2}$ $\eta=0.95$

TABLE 2. Comparison of the Expected Mean Absolute Error (EMAE), convergence order (ECO), and computational time (in seconds) for Example 4.1 ($\mathcal{J}^{\eta}_{0,t}x(t)+\sigma\omega(t)$) using the IQS- [33] and developed combined algorithms. Parameters are set to $\eta\in(0.5,2)$, $\sigma=\frac{1}{\pi^2}$ and $\delta=\{0.02,0.01,0.005\}$ over the interval $t\in[0,3]$.

		IQS-algorithm [33]			Developed combined algorithm		
β	δ	EMAE	ECO	$CPUtime$	EMAE	ECO	$CPUtime$
0.6	0.02	7.89×10^{-3}	1.24	2.016	8.67×10^{-6}	3.00	1.218
	0.01	3.91×10^{-3}	1.20	7.312	6.67×10^{-7}	3.09	4.844
	0.005	1.97×10^{-3}	1.18	32.250	1.67×10^{-7}	2.95	22.813
0.95	0.02	8.05×10^{-3}	1.23	2.000	4.20×10^{-5}	2.59	1.109
	0.01	3.98×10^{-3}	1.20	7.281	4.00×10^{-6}	2.70	4.953
	0.005	1.96×10^{-3}	1.18	31.984	1.67×10^{-7}	2.95	22.906
1.6	0.02	7.29×10^{-3}	1.26	1.984	1.60×10^{-5}	2.82	1.171
	0.01	3.63×10^{-3}	1.22	7.125	4.33×10^{-6}	2.68	4.922
	0.005	1.80×10^{-3}	1.19	32.735	7.22×10^{-7}	2.66	23.000
1.95	0.02	6.60×10^{-3}	1.29	1.844	2.15×10^{-5}	2.74	1.218
	0.01	3.29×10^{-3}	1.24	7.407	6.00×10^{-6}	2.61	4.969
	0.005	1.62×10^{-3}	1.22	31.797	1.67×10^{-6}	2.51	23.172

FSD-HIV-1 model is expressed as

$$\begin{cases} {}^{C}\mathscr{D}^{\eta_1}_{0,t}y(t)=\chi y(t)\left(1-\frac{y(t)}{K}\right)-\phi y(t)-Py(t)z(t)+\sigma_1 y(t)\frac{d\omega_1(t)}{dt}, \\ {}^{C}\mathscr{D}^{\eta_2}_{0,t}z(t)=\frac{\varrho y(t-\theta)z(t-\theta)}{1+hy(t-\theta)}-qy(t)z(t)-\varphi z(t)+\sigma_2 z(t)\frac{d\omega_2(t)}{dt}, \\ y(t)=y_0, \qquad z(t)=z_0, \qquad\qquad t\in[-\theta,0], \end{cases} \tag{4.4}$$

where $\eta_1,\eta_2\in(0.5,1)$. Explanations of symbols are provided in below. Moreover, the estimated parameter values and their references are given in Table 3.

TABLE 3. Estimated parameter values and their references.

Parameter	Estimated Value	Cite
y_0	0.001	[13]
z_0	144	[27]
χ	22.6740	[27]
K	1832.4021	[27]
P	1.7592×10^{-4}	[27]
ϱ	0.1790	[27]
h	10.2972	[27]
q	4.34×10^{-9} or 0.02	[27]
φ	0.013	[13]
ϕ	22.6	[45]
θ	20.50 or 26.54	[27]
κ	$(0.0370, 0.0329)$	Estimated

Nomenclature		
Parameters	Description	Units
$y(t)$	virus population	$virus\ mm^{-3}$
$z(t)$	Cells associated with the immune response (mainly $CD4^+$ T cells)	$cell\ mm^{-3}$
$\chi \in [2, 50]$	viral replication rate	day^{-1}
$K \in [348, 2500]$	target cell limitation	$virus\ mm^{-3}$
$P \in [0, 1]$	rate of virus killing by immune response	$mm^3 cells^{-1} day^{-1}$
$\varrho \in [0, 100]$	maximum proliferation rate of immune cells	$mm^3 virus^{-1} day^{-1}$
$h \in [0, 15]$	half-saturation constant	$mm^3 virus^{-1}$
$q \in [0, 0.01]$	viral inhibition rate	$mm^3 virus^{-1} day^{-1}$
$\phi y(t)$	the population of virus cleared at a given rate	day^{-1}
φ	immune clearance rate of $CD8^+$ T-cell-dominated and natural mortality rate	day^{-1}
$\theta \in [15, 35]$	Time delay	day
$\sigma, \sigma_2 \in [0.2]$	intensities of Brownian motions	–
$\omega_1(t)$ and $\omega_2(t)$	Two uncorrelated standard Brownian motions	–

In response to concerns about the biological realism of the very small value $q = 4.34 \times 10^{-9}$ (which leads to negligible direct viral killing of immune cells), we have added a simulation with an intermediate inhibition rate $q = 5 \times 10^{-5}$, chosen within the range $[10^{-6}, 10^{-4}]$. The corresponding results are included in the revised Figure 7 and discussed below. These simulations show a gradual transition between near-neutral and strongly immunosuppressive behavior, confirming that realistic dynamics indeed occur at intermediate values. We note that the extremely low q value originates from a specific data-fitting study [27] and should be interpreted cautiously in isolation.

4.2.1. *The impact of intracellular delay (θ) on dynamics.* The intracellular delay indicates that some cells do not respond quickly to the virus entry and need time. Therefore, considering the delay makes the model more realistic. In addition, the delay has a large impact on some important parameters for the antiviral immune response. Therefore, to study the effect of the delay on the dynamics, we mainly deal with changing the delay value based on some known results. As a result, in this subsection, we consider all the parameters of Table 3 with $q = 4.34 \times 10^{-9}$ and $\theta = \{20.50, 26.54\}$ for $\eta_1 = 0.85$ and $\eta_2 = 0.95$. The curves obtained from the numerical solutions of Eq. (4.4) are presented in Figure 3 for different values of the delay in deterministic ($\sigma_1 = \sigma_2 = 0$) and stochastic cases ($\sigma_1 = 0.0370,\ \sigma_2 = 0.0329$) cases with $\delta = 0.05$.

TABLE 4. The SIs approximated values for the 400 simulated trajectories of fractional stochastic system (4.4), with $\eta_1 = 0.85$ and $\eta_2 = 0.95$ for $q = 4.34 \times 10^{-9}$, $\theta_1 = 20.50$, $\theta_2 = 26.54$ and $\delta = 0.02$ at $T = 50$.

	SIs	$\theta_1 = 20.50$	$\theta_2 = 26.54$
$y(t)$	Mean	5.9827×10^{-3}	5.9838×10^{-3}
	Median	5.9950×10^{-3}	5.9961×10^{-3}
	First quartile	5.9352×10^{-3}	5.9364×10^{-3}
	Third quartile	6.0321×10^{-3}	6.0330×10^{-3}
	Skewness	-0.1320	-0.1325
	Kurtosis	2.921	2.921
	Standard deviation	7.1584×10^{-5}	7.1607×10^{-5}
	95% Confidence interval	$[5.8624 \times 10^{-3}, 6.1029 \times 10^{-3}]$	$[5.8635 \times 10^{-3}, 6.1041 \times 10^{-3}]$
$z(t)$	Mean	85.311	85.204
	Median	85.292	85.191
	First quartile	84.550	84.446
	Third quartile	86.124	86.019
	Skewness	0.0549	0.0546
	Kurtosis	2.856	2.858
	Standard deviation	1.0034	1.0016
	95% Confidence interval	[83.625, 86.997]	[83.521, 86.887]

According to Figure 3(top), the time delay affects the peak concentration of the virus. A longer delay leads to a higher peak, although this difference is not very significant. In addition, the shorter the intracellular delay, the shorter the time for the virus to reach the first peak. As shown in Figure 3 (bottom), changing the delay also affects the time to peak. However, changing the delay does not have a significant effect on the concentration of $CD4^+$ T cells. This suggests that the development of viral immunity is not dependent on the time delay. According to the plots presented in Figure 3, in both the deterministic and random cases, HIV-1 viral load and $CD4^+$ T cell count are closely related. When the virus concentration reaches its peak, the $CD4^+$ T cell concentration is at its lowest point at about the same time. This indicates an antagonistic interaction between the virus and immune cells.

The statistical indicators reported in Tables 4 and 5 have been recomputed using 400 independent trajectories (increased from 50 in the original submission). The updated values exhibit greater stability, particularly for skewness and kurtosis, and the 95% confidence intervals are now noticeably tighter. The qualitative conclusions remain unchanged with the larger sample size, while the quantitative estimates are more reliable.

We note that because the FSD-DEs analytical solutions cannot be gained by means of standard mathematical method, so upper 95% confidence interval (CI) is used to predict sample trajectories behavior of approximated solutions in fractional stochastic models [11, 34]. Consequently, the approximated values of the *statistical indicators* (SIs) based on 400 simulated trajectories are represents for $\theta_1 = 20.50$, $\theta_2 = 26.54$ at $T = 50$ in Table 4. According to this table, we observe that

- The resulting diagram of these simulated trajectories aren't symmetric because the mean and second quartile (median) values aren't equal;
- The distributions are platykurtic, as the estimated kurtosis values are less than 3;
- For Skewness> 0, we conclude that the difference between the third and second quartiles is greater than the difference between the second and first quartiles. The opposite result is obtained for Skewness< 0.

4.2.2. *The impact of viral inhibition rate (q) on dynamics.* The immune cells killed by HIV-1 infection are mainly $CD4^+$ T cells. In this subsection, we investigate the effect of the parameter q. For this purpose, we consider the values of $q = 4.34 \times 10^{-9}$ and $q = 0.002$. The other parameters are based on the values given in Table 3. It is worth noting

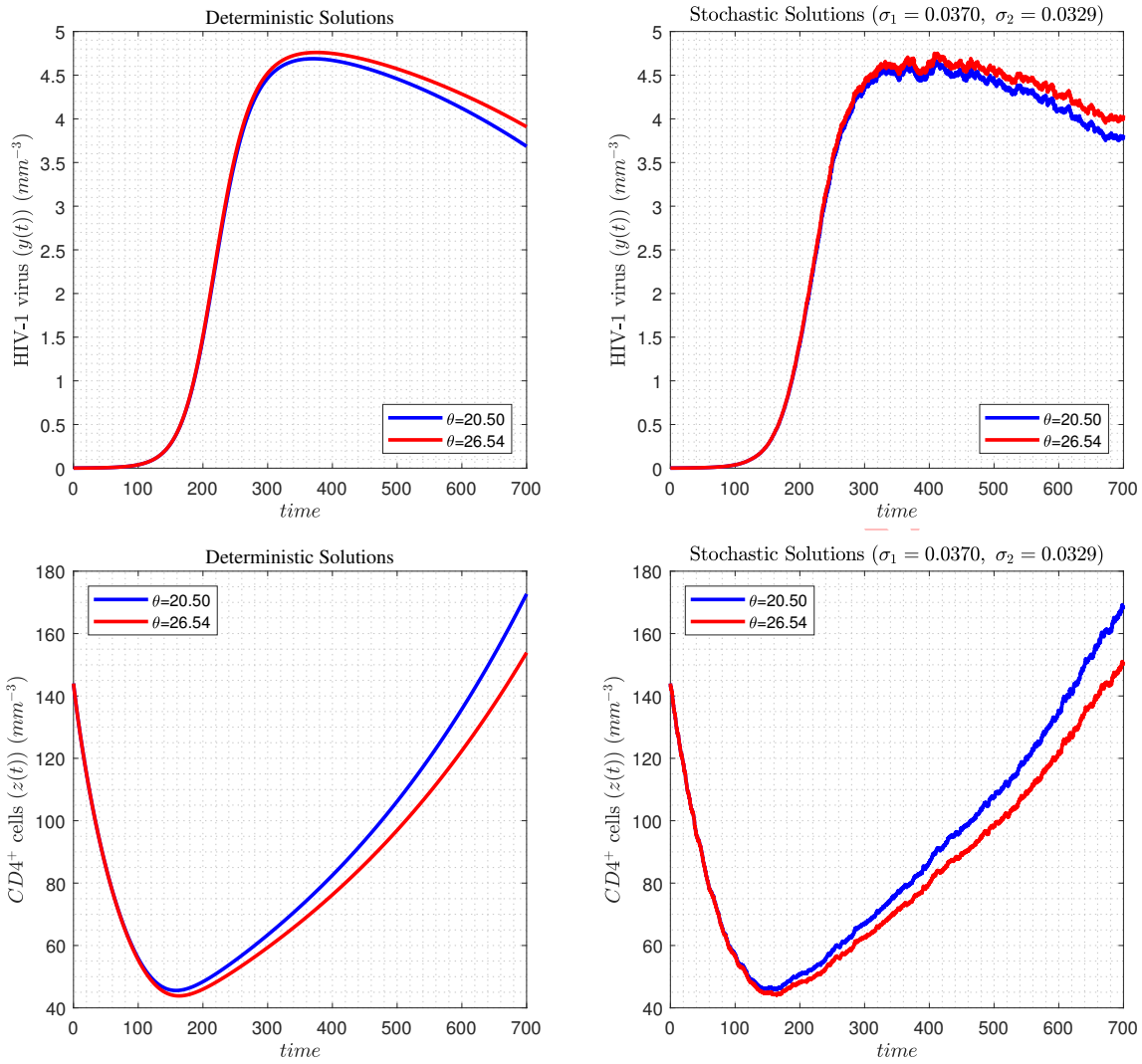

FIGURE 3. Numerical results of concentration variation graphs of HIV-1 (top) and CD4$^+$ T cells (bottom) in Eq. (4.4) for deterministic and stochastic cases, with $\theta = 20.50$ and $\theta = 26.54$ for $q = 4.34 \times 10^{-9}$, $\delta = 0.05$, $\eta_1 = 0.85$ and $\eta_2 = 0.95$.

that we take $\eta_1 = 0.85$ and $\eta_2 = 0.95$ and intracellular delay for $\theta = 26.54$. The results of the numerical simulations for $\delta = 0.05$ are presented in Figur 4.

According to Figure 4, the change in the concentration of virus and immune cells is relatively small when the viral inhibition rate on immune cells is very low. However, if the rate at which the virus kills immune cells is very high (for $q = 0.002$), this can lead to immune paralysis and destruction of immune cells. As a result, the virus remains. Therefore, after the viral inhibition rate exceeds a certain threshold, immune cells will be unable to control the viral attack, which may have serious effects on the patient's body.

The approximated values of the SIs based on 400 simulated trajectories are represents for $q = 4.34 \times 10^{-9}$ and $q = 0.002$ at $T = 50$ in Table 5. Similar results are presented in Table 4.

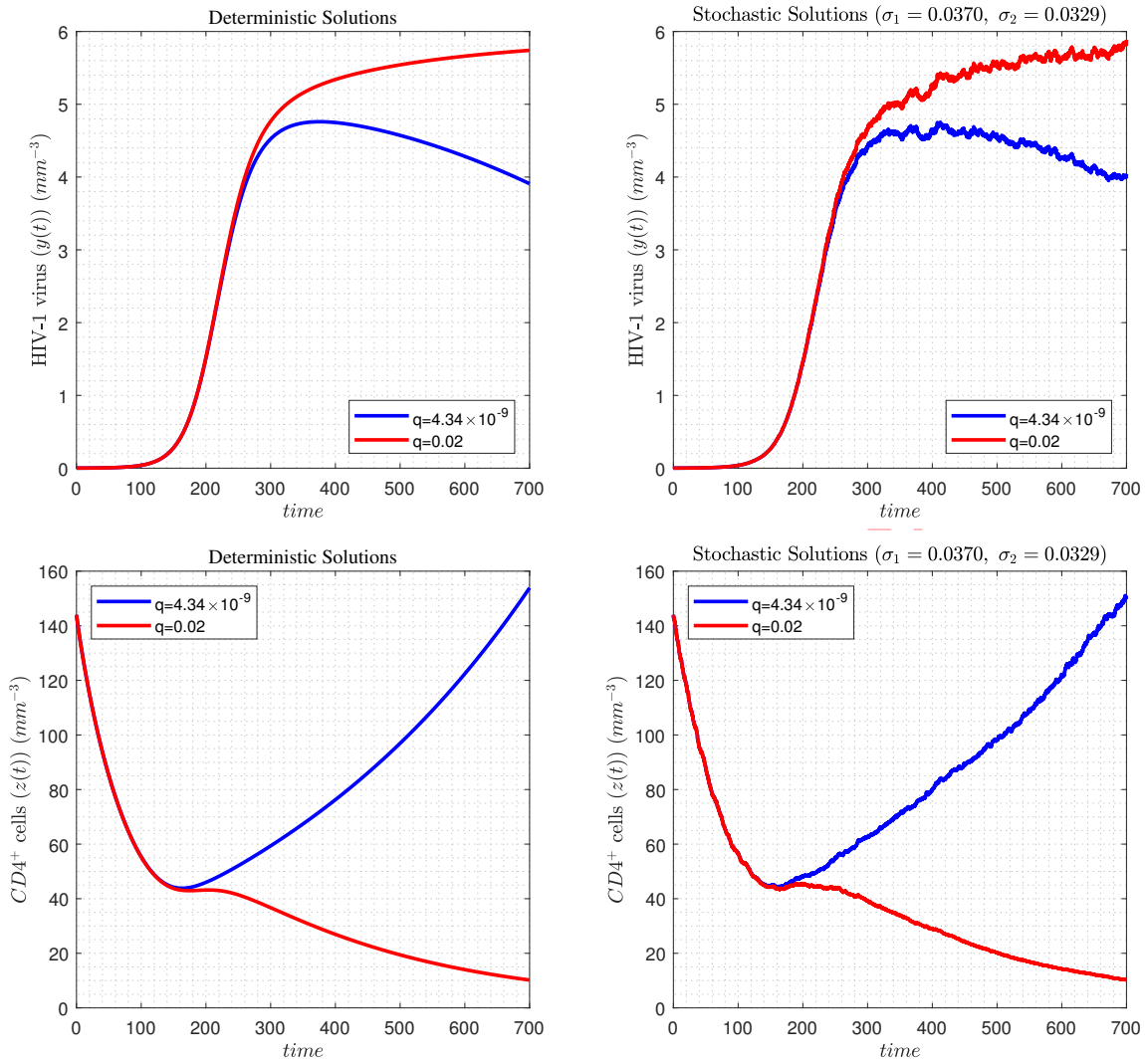

FIGURE 4. Numerical results of concentration variation graphs of HIV-1 (top) and CD4$^+$ T cells (bottom) in Eq. (4.4) for deterministic and stochastic cases, with $q = 4.34 \times 10^{-9}$ and $q = 0.002$ for $\theta = 20.50$, $\delta = 0.05$, $\eta_1 = 0.85$ and $\eta_2 = 0.95$.

5. Conclusion

This study presents a combined algorithm based on linear and quadratic interpolations for approximating fractional integrals, where the linear and quadratic interpolations utilize B-spline and Lagrange functions, respectively. We have rigorously established the error and convergence analysis of this method, demonstrating its theoretical soundness. Furthermore, this combined algorithm serves as an explicit computational framework for calculating approximate solutions of fractional stochastic delay differential equations (FSD-DEs).

The performance of the proposed algorithm has been validated through numerical experiments involving the approximation of fractional integrals of test functions. The method demonstrates significant advantages in terms of accuracy, convergence order, and computational time when compared with existing approaches, such as the integro

TABLE 5. The SIs approximated values for the 400 simulated trajectories of fractional stochastic system (4.4), with $\eta_1 = 0.85$ and $\eta_2 = 0.95$ for $\theta = 26.54$, $q_1 = 4.34 \times 10^{-9}$, $q_2 = 0.002$, and $\delta = 0.02$ at $T = 50$.

	SIs	$q_1 = 4.34 \times 10^{-9}$	$q_2 = 0.002$
$y(t)$	Mean	5.9838×10^{-3}	5.9842×10^{-3}
	Median	5.9961×10^{-3}	5.9963×10^{-3}
	First quartile	5.9364×10^{-3}	5.9371×10^{-3}
	Third quartile	6.0330×10^{-3}	6.0342×10^{-3}
	Skewness	-0.1325	-0.1326
	Kurtosis	2.921	2.921
	Standard deviation	7.1607×10^{-5}	7.1612×10^{-5}
	95% Confidence interval	$[5.8635 \times 10^{-3}, 6.1041 \times 10^{-3}]$	$[5.8638 \times 10^{-3}, 6.1045 \times 10^{-3}]$
$z(t)$	Mean	85.204	85.184
	Median	85.191	85.172
	First quartile	84.446	84.435
	Third quartile	86.019	85.990
	Skewness	0.0546	0.0545
	Kurtosis	2.858	2.858
	Standard deviation	1.0016	1.0014
	95% Confidence interval	[83.521, 86.887]	[83.502, 86.866]

quadratic spline (IQS) algorithm. Subsequently, we applied the explicit method to investigate a fractional HIV-1 infection model incorporating random fluctuations and time delays. Through systematic analysis under various scenarios of intracellular delay and viral inhibition rates, we examined the stochastic impacts on the FSD HIV-1 infection model dynamics. The study revealed that HIV-1 viral load and $CD4^+$ T cell count exhibit a closely coupled yet inversely related behavior, where peak viral concentration coincides temporally with the minimum $CD4^+$ T cell concentration, thereby indicating a clear antagonistic interaction between the virus and immune cells.

Statistical indicators were employed to assess the performance of the combined algorithm across multiple simulated trajectories, providing comprehensive insights into the method's reliability and stability. The numerical results reveal the feasibility and robustness of the combined algorithm across various fractional orders, confirming its capability to handle complex dynamics in fractional stochastic systems. The findings demonstrate that the proposed approach enables effective graphical visualization and numerical comparison of different FSD-DEs, particularly in biomedical applications where memory effects, time delays, and stochastic perturbations play crucial roles. This methodology opens new avenues for investigating complex phenomena in the medical field and other domains where fractional calculus provides a more accurate representation of system dynamics than classical integer-order models.

DECLARATIONS

Ethical Approval. Not applicable. This study is theoretical and computational in nature and does not involve human or animal subjects.

Availability of Supporting Data. No datasets were generated or analyzed during this study, as it focuses on numerical simulations and theoretical analysis. All results are presented within the manuscript.

Competing Interests. The authors, M. Khadem Mohammadi, B. Parsa Moghaddam, A. Yaghobnia, and M. Askaripour Lahiji, declare no competing interests that could influence the research presented in this manuscript.

Funding. No funding was received for this research.

Authors' Contributions. M. Khadem Mohammadi designed the numerical methodology, performed computational experiments, and drafted the manuscript. B. Parsa Moghaddam conceptualized the study, developed the theoretical framework, and critically revised the manuscript. A. Yaghobnia contributed to the convergence analysis, provided technical expertise, and reviewed the manuscript. M. Askaripour Lahiji assisted in the application of fractional calculus to fractional stochastic HIV infection model, refined the theoretical analysis, and revised the manuscript. All authors read and approved the final manuscript.

Acknowledgments. No acknowledgments to report at this time.

References

[1] S. Abdi-mazraeh, S. Irandoust-pakchin, and M. Adel, *The construction of stochastic operational matrix via sparsity properties using B-spline wavelets to solve fractional stochastic integro-differential equations*, International Journal of Dynamics and Control, *13*(5) (2025), 1–14.
[2] D. Adak and N. Bairagi, *Analysis and computation of multi-pathways and multi-delays HIV-1 infection model*, Applied Mathematical Modelling, *54* (2018), 517–536.
[3] R. P. Agarwal, D. Baleanu, J. J. Nieto, D. F. M. Torres, and Y. Zhou, *A survey on fuzzy fractional differential and optimal control nonlocal evolution equations*, Journal of Computational and Applied Mathematics, *339* (2018), 3–29.
[4] F. M. Atay, *Complex time-delay systems: theory and applications*, Springer Science & Business Media, 2010.
[5] N. Ayazi, P. Mokhtary, and B. P. Moghaddam, *Efficiently solving fractional delay differential equations of variable order via an adjusted spectral element approach*, Chaos, Solitons & Fractals, *181* (2024), 114635,
[6] F. G. Bahador, P. Mokhtary, andM. Lakestani, *Mixed Poisson-Gaussian noise reduction using a time-space fractional differential equations*, Information Sciences, *647* (2023), 119417,
[7] S. Banerjee, *Mathematical modeling: models, analysis and applications*, CRC Press, 2014.
[8] M. Caputo, *Linear models of dissipation whose Q is almost frequency independent-II*, Geophysical Journal International, *13*(5) (1967), 529–539.
[9] M. Caputo, *Elasticità e dissipazione*, Zanichelli, Bologna, Italy, 1969.
[10] A. C. Cevikel and E. Aksoy, *Soliton solutions of nonlinear fractional differential equations with their applications in mathematical physics*, Revista Mexicana de Física, *67*(3) (2021), 422–428.
[11] C. Chatfield, *Statistics for technology: a course in applied statistics*, Routledge, 2018.
[12] D. Chowdhury and L. Santen, *A. Schadschneider, Statistical physics of vehicular traffic and some related systems*, Physics Reports, *329*(4-6) (2000), 199–329.
[13] R. V. Culshaw and S. Ruan, *A delay-differential equation model of HIV infection of $CD4^+$ T-cells*, Mathematical Biosciences, *165*(1) (2000), 27–39.
[14] H. B. Fung, E. A. Stone, and F. J. Piacenti, *Tenofovir disoproxil fumarate: a nucleotide reverse transcriptase inhibitor for the treatment of HIV infection*, Clinical Therapeutics, *24*(10) (2002), 1515–1548.
[15] M. Gohar, C. Li, and Z. Li, *Finite difference methods for Caputo–Hadamard fractional differential equations*, Mediterranean Journal of Mathematics, *17*(6) (2020), 194.
[16] J. H. He, *Fractal calculus and its geometrical explanation*, Results in Physics, *10* (2018), 272–276.
[17] S. Irandoust-pakchin, G. R. Zaki, and A. A. J. Akbarfam, *On the inverse problem of time fractional heat equation using Crank-Nicholson type methods and genetic algorithm*, FILOMAT, *38*(19) (2024), 6829–6849,
[18] S. Irandoust-Pakchin and M. H. Derakhshan, *A study on an efficient method based on the mixed finite element scheme for solving a fourth-order time-fractional model involving the Riesz space-fractional derivative of distributed order along with a stability analysis*, Journal of Applied Mathematics and Computing, (2025), 1-24,
[19] T. Jin and X. Yang, *Monotonicity theorem for the uncertain fractional differential equation and application to uncertain financial market*, Mathematics and Computers in Simulation, *190* (2021), 203–221.
[20] S. Kumar, S. Ghosh, R. Kumar, and M. Jleli, *A fractional model for population dynamics of two interacting species by using spectral and Hermite wavelets methods*, Numerical Methods for Partial Differential Equations, *37*(2) (2021), 1652–1672.

[21] M. Lakestani and R. Tuntas, *Efficient Solution for Multi-Delay Fractional Optimal Control Problems via Cubic B-Splines*, Optimal Control Applications and Methods, *46*(6) (2025), 2411-2422,
[22] M. Lakestani and R. Tuntas, *Cubic B-spline approach for solving fractional optimal control problems in the Caputo-Fabrizio sense*, Filomat, *39*(22) (2025), 7849-7865.
[23] M. Lakestani, R. Tuntas, and M. Dehghan, *Constructing efficient bases from B-Spline functions and solving fractional optimal control problems*, Journal of Applied Mathematics and Computing, *72*(3) (2026), 120,
[24] K. A. Lazopoulos, and A. K. Lazopoulos, *Fractional differential geometry of curves and surfaces*, Progress in Fractional Differentiation and Applications, *2*(3) (2016), 169–186.
[25] C. Li, A. Chen, and J. Ye, *Numerical approaches to fractional calculus and fractional ordinary differential equation*, Journal of Computational Physics, *230*(9) (2011), 3352–3368.
[26] H. Li, R. Gao, and C. Zhang, *Evolution of HIV/AIDS prevention and control policies in China: a grounded theory approach*, China CDC Weekly, *6*(1)(2024), 12.
[27] Y. Li, Y. Wei, S. Li, Y. Li, and Z. Peng, *Stochastic HIV-1 infection model with time delay: case study of clinical data*, Journal of Biological Dynamics, *19*(1) (2025), 2553766.
[28] X. X. Liao and X. Mao, *Exponential stability and instability of stochastic neural networks*, Stochastic Analysis and Applications, *14*(2) (1996), 165–185.
[29] X. Mao, *Stochastic differential equations and applications*, Elsevier, 2011.
[30] B. P. Moghaddam, J. A. T. Machado, and H. Behforooz, *An integro quadratic spline approach for a class of variable-order fractional initial value problems*, Chaos, Solitons & Fractals, *102* (2017), 354–360.
[31] B. P. Moghaddam, A. M. Lopes, J. A. T. Machado, and Z. S. Mostaghim, *Computational scheme for solving nonlinear fractional stochastic differential equations with delay*, Stochastic Analysis and Applications, *37*(6) (2019), 893–908.
[32] B. P. Moghaddam, L. Zhang, A. M. Lopes, J. A. T. Machado, and Z. S. Mostaghim, *Sufficient conditions for existence and uniqueness of fractional stochastic delay differential equations*, Stochastics, *92*(3) (2020), 379–396.
[33] B. P. Moghaddam, Z. S. Mostaghim, A. A. Pantelous, and J. A. T. Machado, *An integro quadratic spline-based scheme for solving nonlinear fractional stochastic differential equations with constant time delay*, Communications in Nonlinear Science and Numerical Simulation, *92* (2021), 105475.
[34] B. P. Moghaddam, M. Pishbin, Z. S. Mostaghim, O. S. Iyiola, A. Galhano, and A. M. Lopes, *A Numerical Algorithm for Solving Nonlocal Nonlinear Stochastic Delayed Systems with Variable-Order Fractional Brownian Noise*, Fractal and Fractional, *7*(4) (2023), 293.
[35] P. Mokhtary and F. Ghoreishi, *Error Analysis of the Generalized Jacobi Galerkin Method in Nonlinear Fractional Differential Equations*, Progress in Fractional Differentiation and Applications, *9*(4) (2023), 687-700,
[36] Z. Moniri, B. P. Moghaddam, and M. Z. Roudbaraki, *An efficient and robust numerical solver for impulsive control of fractional chaotic systems*, Journal of Function Spaces, *2023*(1) (2023), 9077924.
[37] Z. Moniri, A. Babaei, and B. P. Moghaddam, *Robust numerical framework for simulating 2D fractional time–space stochastic diffusion equation driven by spatio-temporal noise: L1-FFT hybrid approach*, Communications in Nonlinear Science and Numerical Simulation, *146* (2025), 108791.
[38] Z. Moniri, A. Babaei, and B. Parsa Moghaddam, *Numerical exploration of pollutant transport using stochastic fractional diffusion and Karhunen-Loève expansion*, Iranian Journal of Numerical Analysis and Optimization, *16*(1) (2026).
[39] Z. Moniri, M. A. Zaky, A. Babaei, and B. P. Moghaddam, *Stochastic approaches to uncertainty quantification in fractional drift-flux models with concentration-dependent sources for pollutant dispersion*, Stochastic Environmental Research and Risk Assessment, *40*(2) (2026), 49.
[40] B. Øksendal, *Stochastic differential equations, in: Stochastic differential equations*, Springer, (2003), 65–84.
[41] K. M. Owolabi and A. Atangana, *Analysis and application of new fractional Adams–Bashforth scheme with Caputo–Fabrizio derivative*, Chaos, Solitons & Fractals, *105* (2017), 111–119.
[42] A. Papoulis and S. U. Pillai, *Probability, random variables, and stochastic processes*, Tata McGraw-Hill Education, 2002.
[43] P. E. Protter, *Stochastic differential equations*, Springer, 2005.

[44] H. Qi and X. Meng, *Mathematical modeling, analysis and numerical simulation of HIV: the influence of stochastic environmental fluctuations on dynamics*, Mathematics and Computers in Simulation, *187* (2021), 700–719.
[45] B. Ramratnam, S. Bonhoeffer, J. Binley, A. Hurley, L. Zhang, J. E. Mittler, M. Markowitz, J. P. Moore, A. S. Perelson, and D. D. Ho, *Rapid production and clearance of HIV-1 and Hepatitis C virus assessed by large volume plasma apheresis*, The Lancet, *354*(9192) (1999), 1782–1785.
[46] E. L. Read, A. A. Tovo-Dwyer, and A. K. Chakraborty, *Stochastic effects are important in intrahost HIV evolution even when viral loads are high*, Proceedings of the National Academy of Sciences, *109*(48) (2012), 19727–19732.
[47] S. G. Samko, A. A. Kilbas, and O. I. Marichev, *Fractional Integrals and Derivatives: Theory and Applications*, Gordon & Breach Sci. Publishers, 1993.
[48] L. Shaikhet, *Lyapunov functionals and stability of stochastic functional differential equations*, Springer Science & Business Media, 2013.
[49] A. Singh, B. Razooky, C. D. Cox, M. L. Simpson, and L. S. Weinberger, *Transcriptional bursting from the HIV-1 promoter is a significant source of stochastic noise in HIV-1 gene expression*, Biophysical Journal, *98*(8) (2010), L32–L34.
[50] World Health Organization, *Report on the global action plan on HIV drug resistance 2017–2021*, World Health Organization, 2023.
[51] J. Zhang, M. Zhou, P. Wang, D. Wang, Y. Mi, J. Liu, and F. Cheng, *Temporal trends of clinical characteristics and treatments in people living with HIV at the initiation of antiretroviral therapy—Beijing municipality*, China, 2010–2020, China CDC Weekly, *5*(6) (2023), 131.